



**HAL**  
open science

# A Fluctuation–Dissipation Relation for the Ocean Subject to Turbulent Atmospheric Forcing

Achim Wirth

► **To cite this version:**

Achim Wirth. A Fluctuation–Dissipation Relation for the Ocean Subject to Turbulent Atmospheric Forcing. *Journal of Physical Oceanography*, 2018, 48 (4), pp.831-843. 10.1175/JPO-D-17-0097.1 . hal-01769301

**HAL Id: hal-01769301**

**<https://hal.science/hal-01769301>**

Submitted on 18 Apr 2018

**HAL** is a multi-disciplinary open access archive for the deposit and dissemination of scientific research documents, whether they are published or not. The documents may come from teaching and research institutions in France or abroad, or from public or private research centers.

L'archive ouverte pluridisciplinaire **HAL**, est destinée au dépôt et à la diffusion de documents scientifiques de niveau recherche, publiés ou non, émanant des établissements d'enseignement et de recherche français ou étrangers, des laboratoires publics ou privés.

1 **A fluctuation-dissipation relation for the ocean subject to turbulent**  
2 **atmospheric forcing**

3 Achim Wirth\*

4 *Univ. Grenoble Alpes, CNRS, LEGI, F-38000 Grenoble, France*

5 \*Corresponding author address: Achim Wirth, LEGI, Domaine Universitaire CS 40700, 38058  
6 Grenoble Cedex 9, France  
7 E-mail: achim.wirth@legi.cnrs.fr

## ABSTRACT

8 We establish the fluctuation-dissipation relation for a turbulent fluid layer  
9 (ocean) subject to frictional forcing by a superposed lighter fluid layer (at-  
10 mosphere) in local models of air-sea dynamics. The fluctuation-dissipation  
11 relation reflects the fact that air-sea interaction not only injects energy in the  
12 ocean but also dissipates it. Energy injection and dissipation must therefore be  
13 related. The competition between the two processes determines the oceanic  
14 energy budget in the idealized dynamics considered here. When applying the  
15 fluctuation-dissipation relation to a two-dimensional two-layer Navier-Stokes  
16 model with turbulent dynamics, in the atmosphere and the ocean, coupled by  
17 a quadratic friction law, the friction parameter is estimated within 8% of the  
18 true value, while the estimation of the mass ratio between the atmosphere and  
19 the ocean fails, as the forcing time-scale is not faster than the characteristic  
20 time-scale of the atmospheric dynamics.

## 21 **1. Introduction**

22 It was noted by Einstein (1906) that a Brownian particle in a fluid is subject to two processes,  
23 friction and fluctuations, which are both due to the surrounding fluid and must therefore be related  
24 (see Einstein (1906, 1956), Perrin (2014)). The fluctuation-dissipation relation (fdr) establishes  
25 the connection between the two processes (Barrat and Hansen (2003)). The fdr is a key subject  
26 of non-equilibrium statistical mechanics, it is applied to a large variety of linear and non-linear  
27 models and also to configurations where the “Brownian particle” is some “slow” property of a  
28 system.

29 The case considered here: the dynamics of two two-dimensional layers of fluid, in turbulent  
30 motion, coupled by frictional forces at their interface, is conceptually similar. When the mass  
31 (per unit area) in the lower layer (ocean) is much higher than in the upper layer (atmosphere),  
32 the interactions resemble those of a heavy Brownian particle surrounded by light molecules. The  
33 atmospheric velocities are higher and vary more rapidly than the oceanic velocities. Based on this  
34 observation we extend the theory of a Brownian particle forced by collisions with molecules, to the  
35 case of the ocean forced by the atmosphere. The principal difference between the two cases is that  
36 the first is conservative and the second forced and dissipative. Energy and momentum is conserved  
37 when molecules and Brownian-particles collide, this leads to an equipartition of energy between  
38 all the particles involved, molecules and Brownian particles alike (see e.g. Einstein (1906)). When  
39 the wind blows over the ocean the total momentum of the air-sea system is conserved but most of  
40 the mechanical energy of the fluid flow is dissipated to heat in the friction process (see e.g. Moulin  
41 and Wirth (2016)). As a consequence we can not expect equipartition of energy between the  
42 ocean and the atmosphere. Equipartition is the corner stone of the fdr for Brownian motion, in the  
43 case of a dissipative system something else has to stand in lieu of. The theory of the fluctuation-

44 dissipation relation has been extended and applied to forced dissipative dynamical systems far  
45 from equilibrium, for a comprehensive review I refer the reader to Marconi et al. (2008).

46 The problem presented here is one of non-equilibrium thermodynamics. Not only in the sense  
47 that the system evolves from one thermodynamic equilibrium state to another or that it considers  
48 the convergence of a perturbed system towards an equilibrium state. The system considered here  
49 is constantly forced and ensemble averages are evolving, it is in a statistically non-stationary state.

50 As in the case of Brownian motion, the fluctuations and the dissipation of the ocean dynamics  
51 is due to the same process: in air-sea interaction it is the friction between the ocean and the  
52 atmosphere. When the friction law is linear (Rayleigh friction, with a constant coefficient) the  
53 friction time does neither depend on the horizontal structure nor the strength of the current. For  
54 the ocean layer forced by a varying atmosphere the time evolution of the momentum is governed  
55 by the shear between the atmosphere and the ocean and described by the first-order linear ordinary  
56 differential-equation:

$$\partial_t \mathbf{u}_o = S(\mathbf{u}_a - \mathbf{u}_o), \quad (1)$$

57 where  $\mathbf{u}_a$  and  $\mathbf{u}_o$  represent the two-dimensional (horizontal) velocity vectors at a point in the two  
58 dimensional (horizontal) domain or the averaged velocity in a given horizontal domain of the  
59 atmosphere and the ocean layers, respectively. From the above equation we see the double role  
60 of friction between the two layers, it drives the motion in the ocean, through  $S\mathbf{u}_a$  and it dissipates  
61 through  $-S\mathbf{u}_o$ . When the forcing is constant in time the ocean velocity converges exponentially  
62 to the atmospheric velocity with the characteristic friction time of  $S^{-1}$ . When the forcing is much  
63 faster than the friction time, as it is usually the case when the “slow” ocean is forced by a “fast”  
64 atmosphere, eq. (1) is a Langevin equation (see appendix A, e.g. Barrat and Hansen (2003)), if the  
65 atmospheric dynamics is modelled by a stochastic process. The inverse friction time of an ocean

66 surface layer of depth  $D=10\text{m}$  subject to a wind forcing with  $u_{10} = 10\text{m/s}$  (atmospheric speed 10m  
67 above the sea-surface) is roughly a few days  $S = c_d u_{10} \rho_{air} / (\rho_{water} D) \approx (10\text{day})^{-1}$ , where  $\rho$ . are  
68 the densities of the air and the seawater and  $c_d = 10^{-3}$  is the surface drag coefficient. This time  
69 scale is slower than the atmospheric dynamics over a large range of scales. For further information  
70 on the dynamics in the planetary boundary layer and the friction over the ocean I refer the reader  
71 to Stull (2012), for the ocean mixed layer to Vallis (2017) and for air-sea interaction to Csanady  
72 (2001).

73 In the above Langevin equation the first term gives the fluctuating force due to the chaotic  
74 dynamics of the atmosphere and the second term the dissipation by friction of the ocean at the in-  
75 terface. The first is random while the second is systematic, but both have the same origin and must  
76 therefore be related. This relationship is usually referred to as the fluctuation dissipation *relation*  
77 (fdr) (see e.g. Barrat and Hansen (2003)) and will be established here for air-sea interaction. The  
78 fluctuation dissipation *theorem* compares the response of a system subject to an external distur-  
79 bance to the internal fluctuations of the unperturbed system and will be considered elsewhere.

80 By using eq. (1) we neglect the horizontal exchange of momentum for the point considered or  
81 through the horizontal boundary of the domain, when the variables present domain averages. The  
82 importance of fluxes through the interface with respect to horizontal fluxes through the domain  
83 boundary increases linearly with domain size, as the circumference of a domain grows linearly  
84 with its size and the surface area quadratically. We further suppose that in our two-dimensional  
85 layer the horizontal friction is small enough so that the dissipation of energy by horizontal friction  
86 at small scales can be neglected. This is due to the inverse energy cascade of two-dimensional  
87 turbulence, which leads to smaller horizontal energy-dissipation for smaller viscosities (Boffetta  
88 and Ecke (2012)). If the viscosity is small enough the energy dissipation is dominated by the  
89 friction at the atmosphere-ocean interface.

90 When the energy in the ocean layer is considered, eq. (1) multiplied by  $\mathbf{u}_o$ , we see that the  
91 covariance between the velocities in both layers  $\langle \mathbf{u}_a \cdot \mathbf{u}_o \rangle_A$  determines the energy input over a  
92 domain  $A$ .

93 There is, however, an important difference to the classical Langevin equation, as the forcing by  
94 the atmospheric velocity at time  $t_o$  has some dependence on the ocean velocity at previous times  
95  $t < t_o$ . Mathematically speaking, the process is non-Markovian, when only the ocean dynamics  
96 is considered. The correlation is such that the ocean does not reach a statistically stationary state.  
97 To take this important difference into account we consider the atmosphere-ocean system coupled  
98 by friction at the sea surface and subject to an external forcing, rather than the ocean subject to an  
99 atmospheric forcing. The governing equations (eqs. (2), (3)) are given in the next section.

100 We will show that the fdr relates the velocity correlations in and between both layers. We also  
101 extend the fdr to a quadratic friction law between the atmosphere and the ocean. In this case  
102 the friction time is a function of the shear. We finally use the results from the local models, that  
103 have no horizontal extension, to apply the fdr to the case of a fine-resolution two-dimensional  
104 Navier-Stokes model for both, the atmosphere and the ocean, with a turbulent dynamics on a large  
105 range of horizontal scales. To explore the role of the fdr in air-sea-interaction we here work with  
106 a hierarchy of three models: a linear-friction and a quadratic-friction local model and a quadratic-  
107 friction two-dimensional Navier-Stokes model.

108 The foundation of stochastic climate dynamics was laid by Hasselmann (1976) and Frankig-  
109 noul and Hasselmann (1977). Research on idealized models of the coupled air-sea system has  
110 been performed in recent years: Hogg et al. (2003) considered the dynamics of two superposed  
111 quasi-geostrophic models (one for the ocean and one for the atmosphere and both giving rise to a  
112 turbulent dynamics) interacting through mixed layer models. In their simulations heat exchange  
113 is bi-directional but the ocean velocities are not used in determining the exchange of momentum

114 at the air-sea interface. In the here presented work, there is no heat exchange and the momentum  
115 exchange is a function of the difference of the velocities between the atmosphere and the ocean.  
116 Using this physically consistent way of calculating the momentum exchange was found to lead to  
117 significant changes in the ocean dynamics Duhaut and Straub (2006), who used a constant-in-time  
118 prescribed wind-stress. It was furthermore demonstrated by by Beena and Von Storch (2009) that  
119 fast variability in the air-sea forcing has an important effect on the ocean circulation at large scales.  
120 This work was later extended to a coupled climate model with a stochastic term in the air-sea in-  
121 teraction by Williams (2012). In the present work I consider highly idealized models based on  
122 stochastic differential equations, which can be solved analytically, are used to analyse simulations  
123 of two dimensional models of interacting air-sea dynamics, where the variability is a result of the  
124 internal turbulent dynamics, only. I extend the fdr derived for the local sde to the two-dimensional  
125 turbulent deterministic model of air-sea interaction.

126 By considering air-sea dynamics as one system, rather than the sea subject to an atmospheric  
127 forcing, has shown, in previous work, to give rise to a new instability mechanism (Moulin and  
128 Wirth (2014)) and new dynamical behavior (Moulin and Wirth (2016)). The present work aims  
129 at considering the air-sea-system in the simplest possible model having a dynamics over a large  
130 range of space and time scales. The effect of a rotating frame (Coriolis force) which is key to large-  
131 scale oceanic flow and air-sea interaction is not considered here. The important process of heat  
132 fluxes at the interface is not included, it is conceptually similar to the exchange of momentum and  
133 the same formalism can be applied. (Hasselmann (1976) and Frankignoul and Hasselmann (1977)  
134 considered heat, rather than momentum exchange). The purpose of the present work is to introduce  
135 the tools of non-equilibrium statistical mechanics, as stochastic differential equations and Fokker-  
136 Planck equations, in the field of air-sea interaction and to develop the basis of a hierarchy of  
137 models for air-sea interaction. Understanding the non-linear interactions of the ocean and the

138 atmosphere through a large variety of processes over an extended range of scales in time and  
 139 space, asks for a hierarchy of models spanning the wide range from analytically solvable equations  
 140 to comprehensive climate general circulation models (GCMs).

## 141 **2. Local interaction models**

142 A horizontal domain in the ocean exchanges energy with the atmosphere at its surface, but also  
 143 with the surrounding ocean. As the circumference of a domain grows linearly with its size and  
 144 the surface area quadratically, the influence of the interactions at the surface will dominate over the  
 145 lateral fluxes at the boundary, when the domain is large enough.

### 146 *a. Linear model*

147 The turbulent friction at the atmosphere-ocean interface is commonly modelled by a quadratic  
 148 friction law, where the friction force is a constant times the product of the shear speed and the  
 149 shear velocity (see e.g. Stull (2012)). The linear version with a constant eddy-coefficient allows for  
 150 analytic solutions. It is also sometimes used in numerical simulations of the climate dynamics. The  
 151 friction coefficient represents an average (in time and space) mimicking the real friction process.

152 The mass of the atmosphere per unit area is set to unity. The mass of the ocean per unit area  
 153 is  $m$  times the mass of the atmosphere, the total mass per unit area is  $M = m + 1$ . The governing  
 154 equations at each horizontal point, or of an average over a horizontal area, are:

$$\partial_t \mathbf{u}_a = -Sm(\mathbf{u}_a - \mathbf{u}_o) + \mathbf{F} \quad (2)$$

$$\partial_t \mathbf{u}_o = S (\mathbf{u}_a - \mathbf{u}_o) \quad , \quad (3)$$

155 where  $S$  is the inverse of the friction time in the ocean. When a linear model is used ( $S=\text{const}$ )  
 156 both horizontal directions are un-coupled and the problem can be considered independently for  
 157 each direction and we can restrict to studying a one dimensional problem. We therefore employ

158 scalar variables in this subsection. The conservation of total momentum (atmosphere plus ocean)  
 159 sets the inverse friction time for the atmosphere to  $Sm$ . We set  $u_s = u_a - u_o$ , which is the shear  
 160 mode and  $u_t = u_a + mu_o$ , which is the total inertia. Their dynamics is described by two decoupled  
 161 linear equations:

$$\partial_t u_s = -SMu_s + F \quad (4)$$

$$\partial_t u_t = F. \quad (5)$$

162 When the forcing is periodic in time  $F(t) = \cos(\omega t)$  the dynamics is periodic and time averages  
 163  $\langle \cdot \rangle_t$  of second order moments give (see appendix B):

$$\frac{\langle u_a^2 \rangle_t}{\langle u_o^2 \rangle_t} = \frac{\omega^2 + S^2}{S^2} \quad (6)$$

$$\langle u_o^2 \rangle_t = \langle u_a u_o \rangle_t \quad (7)$$

164 When the forcing is delta-correlated-in-time and Gaussian, the statistical properties are com-  
 165 pletely defined by first and second order moments in the linear model. The dynamics is not statis-  
 166 tically stationary and time averages are prohibited, as they depend on the length of the averaging  
 167 interval. Averages are therefore taken over an ensemble ( $\omega \in \Omega$ ) of realizations of forcing func-  
 168 tions  $F_\omega$  and are denoted by  $\langle \cdot \rangle_\Omega$ . Where  $\omega$  is a realization out of the sample space  $\Omega$ , which is the  
 169 set of all possible outcomes. For convenience we suppose that initially ( $t_0 = 0$ ) the dynamics starts  
 170 from rest. The shear mode is the solution of a linear Langevin equation leading to an Ornstein-  
 171 Uhlenbeck process with zero mean and finite second order moment. The total inertia performs a  
 172 centered Random walk, leading to a linear growth of its second order moment. The solution of  
 173 the dynamics in the ocean and atmosphere is a linear combination of the shear mode and the total

174 inertia. The solutions are:

$$u_s(t) = \int_0^t e^{SM(t'-t)} F(t') dt' \quad (8)$$

$$u_t(t) = \int_0^t F(t') dt'. \quad (9)$$

$$\begin{aligned} u_a(t) &= \frac{1}{M}(u_t + mu_s) \\ &= \frac{1}{M} \left( \int_0^t F(t') dt' + m \int_0^t e^{SM(t'-t)} F(t') dt' \right) \end{aligned} \quad (10)$$

$$\begin{aligned} u_o(t) &= \frac{1}{M}(u_t - u_s) \\ &= \frac{1}{M} \left( \int_0^t F(t') dt' - \int_0^t e^{SM(t'-t)} F(t') dt' \right). \end{aligned} \quad (11)$$

175 Using stochastic calculus (see appendix C) we obtain:

$$\begin{aligned} \langle u_a^2 \rangle_\Omega &= \\ \frac{R}{M^2} \left( 2t + \frac{4m}{SM} (1 - e^{-SMt}) + \frac{m^2}{SM} (1 - e^{-2SMt}) \right) \end{aligned} \quad (12)$$

$$\begin{aligned} \langle u_o^2 \rangle_\Omega &= \\ \frac{R}{M^2} \left( 2t - \frac{4}{SM} (1 - e^{-SMt}) + \frac{1}{SM} (1 - e^{-2SMt}) \right) \end{aligned} \quad (13)$$

$$\begin{aligned} \langle u_a u_o \rangle_\Omega &= \\ \frac{R}{M^2} \left( 2t + \frac{2(m-1)}{SM} (1 - e^{-SMt}) - \frac{m}{SM} (1 - e^{-2SMt}) \right). \end{aligned} \quad (14)$$

176 The parameter  $R$  measures the strength of the delta-correlated fluctuating force, it is:

$$2R = \int_{-\infty}^{\infty} \langle F(0)F(t') \rangle_\Omega dt'. \quad (15)$$

177 These equations are rich in information: expanding the above equations in a Taylor series we see  
178 that the initial growth of the square velocity in the atmosphere is linear in time, while it is cubic

179 for the ocean and quadratic for the covariance between the atmospheric and oceanic velocity:

$$\langle u_a^2 \rangle_\Omega = 2Rt + O(t^2) \quad (16)$$

$$\langle u_o^2 \rangle_\Omega = \frac{2RS^2}{3}t^3 + O(t^4) \quad (17)$$

$$\langle u_a u_o \rangle_\Omega = RS t^2 + O(t^3) \quad (18)$$

180 The diffusive growth of the total inertia mode and the boundedness of the shear mode lead to a  
 181 constant and equal growth rate of the square velocity in the atmosphere, the ocean and the covari-  
 182 ance between the atmosphere and ocean velocity, for  $t \gg (SM)^{-1}$ . This resembles equipartition  
 183 of Brownian motion, here not the average energy is constant and equal but the average increase of  
 184 square velocity.

185 The energy balance in the ocean is (using eq. (13) and (14)):

$$\frac{1}{2} \partial_t \langle u_o^2 \rangle_\Omega = S \langle u_a u_o - u_o^2 \rangle_\Omega = \frac{R(1 - e^{-SMt})^2}{M^2}. \quad (19)$$

186 Showing again that, after the initial phase of  $(SM)^{-1}$ , the square velocity in the ocean converges  
 187 to a linear growth rate of  $2RM^{-2}$ , independent of the friction parameter ( $S$ ). Equation (19) also  
 188 connects eqs. (13) and (14) to the time derivative of eq. (13).

189 We then deduce that for  $t \gg (SM)^{-1}$  the following variables are related:

$$\langle (u_a - u_o)^2 \rangle_\Omega = \frac{R}{SM} \quad (20)$$

$$\langle u_a^2 - u_o^2 \rangle_\Omega = \frac{R(M+2)}{SM^2} \quad (21)$$

$$\langle u_a u_o - u_o^2 \rangle_\Omega = \frac{R}{SM^2}. \quad (22)$$

190 From the above equations it is clear that by observing the fluctuations in the atmosphere, the  
 191 ocean and their covariances we can determine  $S$ ,  $R$  and  $M$ .

192 Writing the different terms of eq. (19) in the long-term limit we get:

$$\frac{1}{2} \partial_t \langle u_o^2 \rangle_\Omega = \frac{SR}{M^2} \left( \underbrace{2t + \frac{m-2}{SM}}_{\text{fluctuation}} - \underbrace{2t + \frac{3}{SM}}_{\text{dissipation}} \right) = \frac{R}{M^2}. \quad (23)$$

193 The first two terms in the parenthesis describe the effect of the atmospheric fluctuations that force  
 194 the ocean, while the last two terms are due to dissipation. This can be seen by introducing eqs.  
 195 (13), (14) into eq. (19). Both are related through the equal constant growth-rate of the atmospheric  
 196 and oceanic square velocities and their covariance. One clearly sees that the first and third term,  
 197 which come from the total-inertia mode in the atmosphere and the ocean, respectively, cancel.  
 198 This is due to the fact, that the total inertia mode performs a random walk (Wiener-process) and  
 199 no shear is associated to it. The second and fourth term come from the shear-mode in the atmosphere  
 200 and the ocean, respectively, it converges to a statistically stationary state, an Ornstein-Uhlenbeck  
 201 process. The difference between the fluctuating force and the dissipation leads to a constant-  
 202 in-time increase of the square velocity of the ocean. Although eq. (23) appears tautological, it  
 203 exhibits the balance between fluctuation-dissipation and energy growth. This constitutes a form  
 204 of a (double) fluctuation-dissipation relation, as the dissipation and the fluctuation are related by  
 205 (i) the equal growth rate of their squares and (ii) by the offset between the two. In the case  
 206 of Brownian motion there is equipartition of energy between molecules and Brownian particles,  
 207 which is here replaced by the equal growth rate of the square velocities in the atmosphere, the  
 208 ocean and their covariance. Their intersect values (second and fourth term in the parenthesis) are  
 209 related through the mass difference per unit area ( $m$ ).

### 210 *b. Quadratic models*

211 When the quadratic friction law is used, parameterizing the momentum exchange by turbulent  
 212 boundary layers, both horizontal directions are coupled and a single variable can no longer be

213 used. The governing equations in two dimensional vector notation are:

$$\partial_t \mathbf{u}_a = - \tilde{S} m |\mathbf{u}_s| \mathbf{u}_s + \mathbf{F} \quad (24)$$

$$\partial_t \mathbf{u}_o = \tilde{S} |\mathbf{u}_s| \mathbf{u}_s \quad (25)$$

214 with  $\mathbf{u}_s = \mathbf{u}_a - \mathbf{u}_o$  (bold letters design 2D vectors and  $|\mathbf{u}|$  denotes the absolute value). The forcing  
 215  $\mathbf{F}$  is two-dimensional, delta-correlated-in-time and Gaussian. The forcing in the two components  
 216 is uncorrelated. Note that the model is local, so all (the four scalar) variables depend on time,  
 217 only. Spatial dependence is not considered in this section on local models but will be discussed in  
 218 sections 3 and 4. The stability parameter  $\tilde{S} = c_D L / (Hm)$  is the product of the atmospheric drag  
 219 coefficient the horizontal length scale divided by the atmospheric layer thickness and the mass  
 220 ratio between the ocean and the atmosphere. In the quadratic model the analytic results from the  
 221 previous subsection are no-longer valid, but the governing equations (24) and (25) can still be  
 222 decomposed in a shear part and a total-momentum part, that is eqs. (2) and (3) become:

$$\partial_t \mathbf{u}_s = -\tilde{S} M |\mathbf{u}_s| \mathbf{u}_s + \mathbf{F} \quad (26)$$

$$\partial_t \mathbf{u}_t = \mathbf{F} \quad (27)$$

223 with  $\mathbf{u}_t = \mathbf{u}_a + m \mathbf{u}_o$  (bold letters design 2D vectors). Note that the two modes remain uncoupled  
 224 in the quadratic model, as the total inertia is not changed by the quadratic friction-law, it does not  
 225 depend on the shear and the total inertia does not affect the shear mode. The inverse damping time  
 226 of the shear mode is  $\tilde{S} M |\mathbf{u}_s|$ .

227 The equation for the square velocity of the shear mode is:

$$\frac{1}{2} \partial_t \mathbf{u}_s^2 = -\tilde{S} M |\mathbf{u}_s| \mathbf{u}_s^2 + \mathbf{F} \cdot \mathbf{u}_s. \quad (28)$$

228 When time averages are taken (the shear mode is stationary) we have:

$$\langle \tilde{S} M (\mathbf{u}_s^2)^{3/2} \rangle_t = \langle \mathbf{F} \cdot \mathbf{u}_s \rangle_t = 2R. \quad (29)$$

229 The last equation follows from Stratonovich stochastic calculus (Platen (1999)). When we intro-  
 230 duced in eq. (29) the normalized third order moment of the shear speed:

$$\mu = \frac{\langle (\mathbf{u}_s^2)^{3/2} \rangle}{\langle \mathbf{u}_s^2 \rangle^{3/2}}, \quad (30)$$

231 we obtain that  $\langle \mathbf{u}_s^2 \rangle^{1/2} = (2R/(\mu \tilde{S}M))^{1/3}$ . The factor two appears as the calculations are two-  
 232 dimensional and an independent random-force is applied to both components. We can construct a  
 233 linear Langevin equation with the same second-order moments by introducing the eddy friction

$$\frac{S_{\text{eddy}}}{\tilde{S}} = \frac{\langle (\mathbf{u}_s^2)^{3/2} \rangle}{\langle \mathbf{u}_s^2 \rangle^{3/2}} \langle (\mathbf{u}_s^2)^{1/2} \rangle = \left( \frac{\mu^2 2R}{\tilde{S}M} \right)^{1/3}. \quad (31)$$

234 This means, that the linear eq. (4) with S replaced by  $S_{\text{eddy}}$  has the same first and second-order  
 235 moments as the non-linear equation (26). When we suppose that the components of the velocity  
 236 vector are Gaussian (the pdf of the square-speed is then chi-squared and Weibull) we obtain:

$$\mu_{\text{Gaussian}} = \frac{\langle (\mathbf{u}_s^2)^{3/2} \rangle}{\langle \mathbf{u}_s^2 \rangle^{3/2}} = \frac{3\sqrt{\pi}}{4} \approx 1.3293404. \quad (32)$$

237 In the nonlinear case considered here the dynamics deviates from Gaussian and the actual value can  
 238 be obtained through numerically solving a large ensemble of realizations based on the stochastic  
 239 differential equations.

240 There is, besides the stochastic differential equations approach a second way to study stochastic  
 241 processes: the Fokker-Planck equation. In this approach the object under consideration is the  
 242 probability density function (pdf) and its time evolution in phase space. In the linear case the pdf  
 243 is Gaussian and its evolution completely described by the first and second order moment. In the  
 244 non-linear case this is no-longer true. In appendix D we derive the Fokker-Planck equation for the  
 245 present model and determine the stationary solution of the pdf of the shear mode. This allows to  
 246 determine an analytic solution (using the gamma-function  $\Gamma(x)$ ) of the true value of the normalized

247 third order moment in the stationary case:

$$\mu_{\text{true}} = \frac{2}{3} \left[ \frac{\Gamma(2/3)}{\Gamma(4/3)} \right]^{3/2} \approx 1.2449 \quad (33)$$

248 which is less than 7% lower than the Gaussian value.

### 249 *c. Numerical Results*

250 The linear and non-linear model are integrated numerically (see appendix E), with an ensemble  
251 size of  $10^6$ . Numerical results for the variances of the atmospheric and oceanic velocities and their  
252 covariance presented in the fig. 1, show an almost perfect agreement between the analytic model  
253 (eqs. 12 - 14) and the linear model. They also confirm the validity of the eddy-friction approach,  
254 that is, the second-order moments of the non-linear simulations with ( $M = 101, \tilde{S} = 10^{-3}, R = 0.5$ )  
255 are well fitted by linear integrations with an eddy friction coefficient  $S_{\text{eddy}}$  based on the analytic  
256 value given in eq. (33) and calculated by eq. (31) of  $S = 2.4849 \cdot 10^{-3}$ . The analytic value is for  
257 a stationary pdf and does not apply to the initial adjustment process, this explains the difference  
258 between the numerical experiments and the eddy-friction approach in the initial phase. Numerical  
259 results reveal that the value is independent of  $R$  and  $\tilde{S}$  (not shown).

260 Note that in the linear and the non-linear case we have that: (i) there is a linear growth term  
261 in the energy of the atmosphere, the ocean and in the covariance between the atmospheric and  
262 oceanic velocity; (ii) the energy transfer between the atmosphere and the ocean and the energy in  
263 the ocean does not depend on the friction parameter ( $S$ ).

### 264 **3. Two-dimensional model**

265 We now consider the interaction of two two-dimensional fluid layers in turbulent motion. The  
266 square domain has a side-length of  $l = 10$  and is periodic in both horizontal directions. The two  
267 layers of different mass are coupled through a quadratic friction law. The governing equations for

268 the two components of the velocity fields are:

$$\partial_t \mathbf{v}_i + \mathbf{v}_i \nabla \mathbf{v}_i = \tilde{\mathbf{S}}_i - \nu_i \nabla^4 \mathbf{v}_i + \mathbf{F}_i \quad (34)$$

269 where the two-dimensional field  $\mathbf{v}_i(x, y, t)$  is the local velocity of the atmosphere ( $i = a$ ) and the  
 270 ocean ( $i = o$ ). The friction between the two layers is

$$\tilde{\mathbf{S}}_a = -\tilde{S}m|\mathbf{v}_s|_s \quad (35)$$

$$\tilde{\mathbf{S}}_o = -\tilde{\mathbf{S}}_a/m \quad (36)$$

271 where the subscript  $s$  denotes the shear mode as in the previous section,  $m = 100$  is the mass  
 272 ratio of the oceanic and atmospheric layer and the stability parameter is  $\tilde{S} = 10^{-3}$ . Such value is  
 273 obtained, for example, by an atmospheric friction coefficient of  $c_D = 10^{-3}$  a horizontal length scale  
 274 of  $L = 2 \cdot 10^4$  m, an atmospheric boundary layer thickness of  $H = 2 \cdot 10^2$  m and a 26 m thick ocean  
 275 mixed layer. A particularity of the quadratic drag law is that the balance between the (advective)  
 276 non-linearity and the dissipation does not depend on the fluid speed as both are quadratic. The  
 277 dimensional time scale is given by  $t = L/|\mathbf{v}_s|$ . For a discussion on two-dimensional turbulence  
 278 subject to quadratic dissipation, I refer the reader to Grianik et al. (2004). The external forcing  
 279  $\mathbf{F}_i$  applies only to the atmosphere ( $\mathbf{F}_o = 0$ ), it is such that the vorticity of mode  $k_x = 2\pi 80/L$  is  
 280 fixed. When the vorticity in the forced mode is changed by the turbulent dynamics, the forcing  
 281 restores it instantaneously to the prescribed value. Such kind of forcing has no direct influence on  
 282 all other modes, which can evolve freely. It mimics the effect of the forcing of the flow above the  
 283 atmospheric surface layer which evolves on a slower time scale. The forcing thus happens on the  
 284 internal time-scale of the atmospheric dynamics at the forcing scale and not on a fast time scale  
 285 as in the models discussed above. As the atmosphere evolves on a much faster time-scale than  
 286 the ocean, the forcing of the latter by the former happens on a faster time-scale than the ocean  
 287 dynamics. Such a forcing is also not independent of the atmospheric velocity field. Due to the

288 turbulent dynamics in both layers the forcing is not visible in the snapshots of the vorticity, neither  
289 in the atmosphere nor in the ocean (Fig. 2). It becomes visible in long-term averages.

290 The numerical model used is a pseudo-spectral code of the 2D-Navier-Stokes equations for  
291 both-layers, with 4096 points in both horizontal directions. Integrating the dynamics over a large  
292 range of scales is essential as it allows to reduce the horizontal friction parameter, which leads  
293 to a reduced horizontal energy dissipation. This is due to an energy cascade to large scales in  
294 2D turbulence (see Boffetta and Ecke (2012)). A consequence of this is that energy accumulates  
295 (condensates) at the largest scales of the system where horizontal dissipation is weak, leading  
296 to an increase of energy in the system for a very long time. A difficulty lies in the stiffness of  
297 the problem, ocean speeds are almost two orders of magnitude smaller than their atmospheric  
298 counterparts (see Figs. 2 and 3). The fast atmospheric dynamics at small-scale has to be resolved  
299 over a large time-scale that corresponds to the larger oceanic scales. Few numerical simulations  
300 of the atmosphere-ocean system coupled at every grid point and at every time scale have been  
301 performed so far, exceptions are Moulin and Wirth (2014) and Moulin and Wirth (2016). For  
302 an evaluation of statistical error,  $O(10)$  integrations of the same system have to be performed,  
303 this exceeds the computer resources available to me at present. The numerical time stepping is  
304 performed by a second-order Runge-Kutta scheme with  $\Delta t = 10 \cdot 2^{-18}$ , snapshots are printed every  
305  $\Delta t_{snap} = 10 \cdot 2^{-8}$ . A hyperdiffusive operator is used (see eq. 34) for the horizontal dissipation with  
306  $\nu_a = 4 \cdot 10^{-9}$  and  $\nu_o = 10^{-10}$ .

#### 307 **4. Two-dimensional results**

308 The results presented here correspond to a single numerical experiment over a time interval  
309  $\Delta t_{exp} = 75$  (see Fig. 3), so strictly speaking the ensemble size is one. When the domain is large

310 enough spatial averages can replace ensemble averages as correlations decrease with spatial dis-  
311 tance. In this section the angle brackets  $\langle \cdot \rangle$  denote spatial averages over the entire periodic domain.

312 Horizontal transfers of momentum which are absent in the local models discussed above are  
313 important in the two dimensional dynamics. We will also consider the case when the variables  
314 present averages over horizontal squares, variables are coarse-grained. We therefore define the  
315 vector field  $\mathbf{u}_s = \langle \mathbf{v}_s \rangle_A$  as spatial averages of the local velocities over a domain  $A$ . This coarse-  
316 graining is performed over  $(4096/c)^2$  non-overlapping squares with  $c$  points of side length. For  
317  $c = 1$ ,  $\mathbf{u}_s = \mathbf{v}_s$  as  $A$  corresponds to a single grid-point, and  $\langle \mathbf{u}_s^2 \rangle$  is the average square velocity; for  
318  $c=8$ ,  $\mathbf{u}_s = \langle \mathbf{v}_s \rangle_A$  has  $512^2$  values, each of them being an average over  $8^2$  grid points and  $\langle \mathbf{u}_s^2 \rangle$  is the  
319 average of the square of the  $512^2$  average values. The importance of the exchange of momentum  
320 in the horizontal as compared to the vertical is likely to be smaller when the coarse graining  $c$  is  
321 larger, for the simple geometrical reason that the surface area of the domain considered increases  
322 quadratically, whereas the circumference is a linear function of  $c$ . To quantify the influence of  
323 horizontal momentum exchange I measured the coarse-grained version of the variables.

324 Numerical results from the integrations for different values of the coarse-graining parameter  $c$   
325 are given in tables 1 and 2. In the former the slopes of the best fit regression lines, which are  
326 shown in fig. 3, are given together with their standard deviations. In the latter the differences of  
327 variances and covariances are given, which are stationary following the theory developed for the  
328 linear models. Data from both tables are the basis of the calculation of the friction coefficient and  
329 the mass ratio following the theory developed for the local models. These derived results are given  
330 in table 3, where they are also compared to the actual values.

331 In the two-dimensional calculations the parameters  $\tilde{S}$  and  $M$  are prescribed. When the horizontal  
332 exchange of momentum is neglected we can estimate this parameters based on the velocities in  
333 the ocean and the atmosphere, using the local models. The estimation of the friction coefficient

334  $\tilde{S}$  can be based on the temporal evolution of the averaged square velocity in the linear model, eq.  
 335 (19), with an eddy-friction, or on the non-linear version of the same equation. The estimation of  
 336 the variable  $M$  is based on eqs. (20) and (22), or on the non-linear version of the same equations.

$$S_{\text{obs}} = \frac{\partial_t \langle \mathbf{u}_o^2 \rangle}{2 \langle \sqrt{(\mathbf{u}_a - \mathbf{u}_o)^2} (\mathbf{u}_a \mathbf{u}_o - \mathbf{u}_o^2) \rangle} \quad (37)$$

$$S_{\text{lin}} = \frac{\partial_t \langle \mathbf{u}_o^2 \rangle}{2 \mu_{\text{true}} \sqrt{\langle (\mathbf{u}_a - \mathbf{u}_o)^2 \rangle} \langle (\mathbf{u}_a \mathbf{u}_o - \mathbf{u}_o^2) \rangle} \quad (38)$$

$$M_{\text{obs}} = \frac{\langle ((\mathbf{u}_a - \mathbf{u}_o)^2)^{3/2} \rangle}{\langle (\mathbf{u}_a - \mathbf{u}_o)^2 \rangle^{1/2} \langle (\mathbf{u}_a \mathbf{u}_o - \mathbf{u}_o^2) \rangle} \quad (39)$$

$$M_{\text{lin}} = \frac{\langle (\mathbf{u}_a - \mathbf{u}_o)^2 \rangle}{\langle (\mathbf{u}_a \mathbf{u}_o - \mathbf{u}_o^2) \rangle}. \quad (40)$$

337 The increase of the ocean variance is perfectly fitted by a straight line (see fig. 3) and the co-  
 338 variance between the atmosphere and the ocean is equal to the ocean variance within the statistical  
 339 error, as predicted by the fdr (see fig. 3 and tab. 3). Fluctuations of the atmospheric square-velocity  
 340 are so high that a comparison to the increase of the ocean square-velocity is not possible (see Fig.  
 341 3). Indeed, it is possible to find a time interval over which the slope of the regression line of the  
 342 atmospheric variance equals the one of the ocean.

343 The estimation of the friction parameter  $S$  based on the fdr using the ocean square-velocity  
 344 and the correlation between the ocean and atmospheric velocity are within 10% of the true value  
 345 (tab. 3). There is no significant difference between the local values ( $c = 1$ ) and those of a small  
 346 coarse-graining ( $c = 8$ ) as the smallest resolved features span over 10 grid points, smaller scales  
 347 are well in the dissipation range. For larger coarse graining the estimation of the friction parameter  
 348 diverges.

349 The inverse is true for the estimation of the mass ratio  $M$ , the estimated value is more than a  
 350 decade larger than the true value, for the local data, but seems to converge towards the true value  
 351 for increased coarse-graining.

## 5. Discussion and conclusion

We have analytically derived a *fdr* for a linear local model of air-sea interaction (Rayleigh friction). We showed that the *fdr* can be extended to the non-linear local model (quadratic drag law). Our results with the local models show that the eddy-friction approach is successful as the non-linear model and the linear model with an eddy-friction coefficient (eq. (31)) give similar results and either can be used to analyze the 2D model. Indeed, tab. 3 shows that the estimation of the friction parameter and the mass-ratio are almost identical for both approaches,  $S_{\text{obs}} \approx S_{\text{lin}}$  and  $M_{\text{obs}} \approx M_{\text{lin}}$ . This is important as the friction at an interface is often parameterized using a combination of linear and quadratic friction laws, as the drag-coefficient depends on a variety of processes in a non-linear way. The successful estimation of the friction parameter in the 2-dimensional Navier-Stokes model based on the ocean square-velocity and the covariance of atmospheric and oceanic velocities shows that the *fdr* applies to the ocean dynamics and its forcing by the atmosphere. The estimation of the friction parameter based on eq. (31) is slightly lower than the true value (see tab. 3) as part of the energy is dissipated by horizontal friction. This part decreases when finer resolution and lower (hyper) viscosity is used (see e.g. Boffetta and Ecke (2012)). The divergence of  $S_{\text{eddy/lin}}$  with the coarse graining might be explained by the inverse energy cascade of two-dimensional turbulence. The coarse grained equation neglects the energy input at small scales, not visible in the coarse grained variables, which then cascades to large scales where it becomes visible, leading to an over-estimation of the friction parameter.

In the atmosphere the forcing is created by the dynamics at the forcing scale. Its characteristic time scale  $\tau$  is not fast with respect to the atmospheric dynamics leading to a resonance between the forcing and the atmospheric dynamics and so the estimations  $M_{\text{eddy/lin}}$  are more than a decade larger than the true value. Equations (6) and (7) show that in the case of a periodic forcing the

375 ratio of variances and covariances is governed by the ratio of the forcing frequency to the friction  
376 parameter and is independent of  $M$ . For the Langevin equation to be valid in the atmosphere  
377 and the ocean it is necessary that  $\tau S m \ll 1$  and  $\tau S \ll 1$ , respectively. This explains, why the  
378 approach is more successful to describe the dynamics in the ocean than in the atmosphere. When  
379 coarse graining is increased the situation improves as the eddy-turn-over-time of the atmospheric  
380 dynamics increases with the coarse-graining scale.

381 Presenting the results for coarse-grained variables is not only important from a theoretical point  
382 of view, as observations of the natural system or measurements in the laboratory often include  
383 some degree of coarse-graining. It is also important to note that the values of eddy coefficients  
384 depend on the granularity level.

385 In our model no statistically stationary state is reached as the horizontal friction processes in  
386 the two layers are small, which is a property of high Reynolds number two-dimensional turbulent  
387 flows. The adjustment to a statistically stationary state is thus very slow and exceeds the integration  
388 time of our experiments. In the real atmosphere-ocean boundary layers, the adjustment time might  
389 well be larger than duration of a quasi-stationary forcing (weather system), so that they are not  
390 relevant to the dynamics of the atmosphere and ocean boundary layers. That is, the coupled  
391 boundary layer dynamics is permanently in the process of adjusting to the forcing imposed by  
392 the environment. To explore this non-equilibrium dynamics, the atmosphere-ocean system, rather  
393 than the ocean dynamics subject to atmospheric forcing, has to be considered.

394 We here considered air-sea interaction not only as a source of energy for the ocean but also as a  
395 sink. The balance between the two governs the system. These approaches are new in the field and  
396 allow for establishing the fdr for air-sea interaction.

397 *Acknowledgments.* I am are grateful to Jean-Louis Barrat and Bruno Voisin for discussion. Com-  
 398 ments of two anonymous referees have considerably improved the quality of the paper. LEGI is  
 399 part of Labex OSUG@2020 (ANR10 LABX56).

## 400 APPENDIX A

### 401 Langevin equation

402 For a modern discussion of the Langevin equation we refer to Barrat and Hansen (2003). We  
 403 define the ensemble average  $\langle a(t) \rangle_\Omega$  over realizations  $\omega \in \Omega$  and the time average:

$$\langle a(\tau) \rangle_\tau = \lim_{\tau \rightarrow \infty} \frac{1}{\tau} \int_0^\tau a(t') dt'. \quad (\text{A1})$$

404 When the process is stationary  $\langle a(t) \rangle_\Omega = a$  we can suppose ergodicity (not proven), that is time  
 405 averages and ensemble averages agree  $\langle a(t) \rangle_t = \langle a(t) \rangle_\Omega$ .

406 The Langevin equation is :

$$\partial_t u = -Su + F_\omega. \quad (\text{A2})$$

407 Where  $F_\omega$  is the realization of a random noise (the subscript  $\omega$  is omitted in the sequel). The  
 408 solution:

$$u(t) = e^{-St} u(t_0) + \int_{t_0}^t e^{S(t'-t)} F(t') dt' \quad (\text{A3})$$

$$\begin{aligned} u^2(t) &= e^{-2St} u^2(t_0) + 2u(t_0) \int_{t_0}^t e^{S(t'-2t)} F(t') dt' \\ &+ \int_{t_0}^t \int_{t_0}^t e^{S(t'-t)} e^{S(t''-t)} F(t') F(t'') dt' dt''. \end{aligned} \quad (\text{A4})$$

409 If  $\langle F(t) \rangle_\Omega = 0$  then  $\langle u \rangle_\Omega = e^{-St} u(0)$ . We suppose that  $F(t)$  is stationary and delta correlated in  
 410 time  $2R\delta(t' - t'') = \langle F(t') F(t'') \rangle_\Omega$  where the delta-function has the properties:  $\delta(t - t') = 0$  if

411  $t \neq t'$  and  $\int_{-\infty}^{\infty} \delta(t) dt = 1$ . We have:

$$\begin{aligned}
\langle u^2(t) \rangle_{\Omega} &= e^{-2S(t-t_0)} u^2(0) \\
&+ \int_{t_0}^t \int_{t_0}^t e^{S(t'+t''-2t)} \langle F(t') F(t'') \rangle_{\Omega} dt' dt'' \\
&= e^{-2S(t-t_0)} u^2(t_0) + 2R \int_{t_0}^t e^{2S(t'-t)} dt' \\
&= e^{-2S(t-t_0)} u^2(t_0) + \frac{R}{S} (1 - e^{-2S(t-t_0)}) dt'.
\end{aligned} \tag{A5}$$

412 In the long term behavior, initial conditions are forgotten, that is, exponentials drop and

$$\langle u^2(t) \rangle_{\Omega} = \frac{R}{S}. \tag{A6}$$

413 This result is known as the fluctuation-dissipation relation (fdr) (see Barrat and Hansen (2003)  
414 page 230), as the energy in the system relates dissipation and the strength of the forcing.

415

## APPENDIX B

416

### Periodic Forcing

417 From eqs. 4 and 5 it follows that

$$\begin{aligned}
u_t(t) &= \frac{\sin(\omega t)}{\omega} \\
u_s(t) &= \frac{\omega \sin(\omega t) + SM \cos(\omega t)}{\omega^2 + (SM)^2}
\end{aligned} \tag{B1}$$

418 which leads to:

$$\begin{aligned}
\langle u_t^2 \rangle_t &= \frac{1}{2\omega^2} \\
\langle u_s^2 \rangle_t &= \langle u_s u_t \rangle_t = \frac{1}{2(\omega^2 + (SM)^2)}
\end{aligned} \tag{B2}$$

419 expressing  $u_a$  and  $u_o$  in terms of  $u_t$  and  $u_s$  (the first equality of eqs. 10 and 11) leads to:

$$\langle u_a^2 \rangle_t = \frac{1}{2(\omega^2 + (SM)^2)} \frac{\omega^2 + S^2}{\omega^2} \quad (\text{B3})$$

$$\langle u_o^2 \rangle_t = \langle u_a u_o \rangle_t = \frac{1}{2(\omega^2 + (SM)^2)} \frac{S^2}{\omega^2}. \quad (\text{B4})$$

420 from which eqs. (6) and (7) follow.

421

## APPENDIX C

422

### Stochastic calculus

423 Below are the equations for a random-walk  $u_R$  and a Ornstein-Uhlenbeck process  $u_O$ , the solu-  
 424 tion of a Langevin equation.

$$\partial_t u_R = F \quad (\text{C1})$$

$$\partial_t u_O = -S u_O + F. \quad (\text{C2})$$

425 Solutions are:

$$u_R(t) = \int_{t_0}^t F(t') dt' \quad (\text{C3})$$

$$u_O(t) = \int_{t_0}^t e^{S(t'-t)} F(t') dt'. \quad (\text{C4})$$

426 It follows that:  $\langle u_R \rangle_\Omega = \langle u_O \rangle_\Omega = 0$ . Second order moments are (note that as processes are Gaussian  
 427 first and second order moments completely determine the stochastic processes):

$$\begin{aligned} \langle u_R^2(t) \rangle_\Omega &= \int_{t_0}^t \int_{t_0}^t \langle F(t') F(t'') \rangle_\Omega dt'' dt' \\ &= 2R(t - t_0) \end{aligned} \quad (C5)$$

$$\begin{aligned} \langle u_R(t) u_O(t) \rangle_\Omega &= \int_{t_0}^t \int_{t_0}^t e^{S(t'-t)} \langle F(t') F(t'') \rangle_\Omega dt'' dt' \\ &= \frac{2R}{S} (1 - e^{S(t_0-t)}) \end{aligned} \quad (C6)$$

$$\begin{aligned} \langle u_O^2(t) \rangle_\Omega &= \int_{t_0}^t \int_{t_0}^t e^{S(t'+t''-2t)} \langle F(t') F(t'') \rangle_\Omega dt'' dt' \\ &= \frac{R}{S} (1 - e^{2S(t_0-t)}). \end{aligned} \quad (C7)$$

428

## APPENDIX D

429

### Fokker-Planck equation

430 The sde approach proceeds by following the path of an ensemble of particles and determine  
 431 the probability that a particle is at a certain location in phase space at a given time. There is  
 432 an alternative description of a stochastic process to the sde, which is based on determining the  
 433 partial differential equation (the Fokker-Planck equation, see e.g. Risken (1996)) that governs the  
 434 evolution of the pdf. When a solution of the Fokker-Planck equation is found the pdf is known  
 435 and all statistical quantities, as e.g. moments can be calculated. The difference between the two  
 436 methods is some how similar to the difference of Lagrangian versus the Eulerian description in  
 437 fluid dynamics Klimontovich (1994).

438 For a given sde the corresponding Fokker-Planck equation can be easily derived. The total  
 439 momentum performs a standard diffusion process in the linear (5) and nonlinear (27) model and  
 440 the corresponding Fokker-Planck equation is the constant coefficient diffusion equation. The shear  
 441 mode in the linear model, governed by the sde (4), performs an Ornstein-Uhlenbeck process.

442 The corresponding Fokker-Planck equation describes the evolution of a Gaussian process with a  
443 variance that converges to a constant value. As in these cases the process is known to be Gaussian  
444 the pdf is determined by the first and second moment and nothing is gained by solving the Fokker-  
445 Planck equation instead of calculating the second order moment based on the solution of the sde.  
446 The situation is different for the shear mode in the non-linear model described by the sde (26),  
447 where the functional form of the pdf is not known apriori and all moments have to be calculated  
448 individually. Obtaining the pdf by solving the Fokker-Planck allows to obtain all the moments by  
449 a simple integration. The Fokker-Planck equation corresponding to the sde (26) is (see e.g. Risken  
450 (1996)):

$$P_s(u_s, v_s, t) = \nabla_{uv} \cdot [\tilde{S}M\mathbf{u}_s u_s P_s(u_s, v_s, t) + R\nabla_{uv} P_s(u_s, v_s, t)] \quad (\text{D1})$$

451 where

$$\nabla_{uv} = \begin{pmatrix} \partial_u \\ \partial_v \end{pmatrix}. \quad (\text{D2})$$

452 When we introduce  $E = u_s^2 + v_s^2$  and suppose that the solution is isotropic in the  $u_s, v_s$ -plane we can  
453 write  $P_s(u_s, v_s, t) = \tilde{p}(E)$  and find the stationary isotropic solution to the Fokker-Planck equation  
454 (D1):

$$\tilde{p}(E) = \frac{\beta^{2/3}}{\Gamma(5/3)} \exp(-\beta E^{3/2}) \quad \text{with} \quad \beta = \frac{\tilde{S}M}{3R} \quad (\text{D3})$$

455 and the gamma function  $\Gamma(x)$ . Straightforward calculations then lead to eq. (33).

## 456 APPENDIX E

### 457 Numerical Integration of the Stochastic Differential Equations

458 Please see Platen (1999) for an introduction to the numerical integration of stochastic differential  
459 equations. For the linear case analytic solutions are known, which can be used to validate the

460 numerics. The stochastic differential equations for eqs. (2) and (3) are:

$$du_a = - Sm(u_a - u_o)dt + F dW \quad (\text{E1})$$

$$du_o = S (u_a - u_o)dt \quad (\text{E2})$$

461 where  $W$  is a Wiener process, its derivative  $dW$  is white in time. The noise is additive and so the  
 462 numerical integration of the SDE is straightforward and there is no space for interpretation, as Itô  
 463 and Stratonovich formalism of the equation agree.

464 For the time stepping  $t = n\Delta t$  use the Euler-Maruyama Method, which is a first order numerical  
 465 scheme weak convergence) when additive noise is used (it is equal to the Milstein method in this  
 466 case, see e.g. Platen (1999):

$$u_a(n+1) = u_a(n) - Sm(u_a(n) - u_o(n))\Delta t + F \zeta(n)\sqrt{\Delta t} \quad (\text{E3})$$

$$u_o(n+1) = u_o(n) + S (u_a(n) - u_o(n))\Delta t. \quad (\text{E4})$$

467 The time-step is  $\Delta t$  and  $\zeta(n)$  is a normally distributed centered random variable with  
 468  $\langle \zeta(n)\zeta(m) \rangle = \delta_{n,m}$ .

469 In the nonlinear case (noise is still additive) the stochastic differential equations are:

$$du_a = - \tilde{S}m\bar{u}_s(u_a - u_o)dt + F_u dW_u \quad (\text{E5})$$

$$dv_a = - \tilde{S}m\bar{u}_s(v_a - v_o)dt + F_v dW_v \quad (\text{E6})$$

$$du_o = \tilde{S} \bar{u}_s(u_a - u_o)dt \quad (\text{E7})$$

$$dv_o = \tilde{S} \bar{u}_s(v_a - v_o)dt \quad (\text{E8})$$

470 where  $W_u$  and  $W_v$  are two independent Wiener processes and  $\bar{u}_s = \sqrt{(u_a - u_o)^2 + (v_a - v_o)^2}$ .

471 The first order numerical scheme is:

$$\begin{aligned} u_a(n+1) = & u_a(n) - \tilde{S}m\bar{u}_s(n)(u_a(n) - u_o(n))\Delta t \\ & + F_u\zeta_u(n)\sqrt{\Delta t} \end{aligned} \quad (\text{E9})$$

$$\begin{aligned} u_a(n+1) = & u_a(n) - \tilde{S}m\bar{u}_s(n)(u_a(n) - u_o(n))\Delta t \\ & + F_v\zeta_v(n)\sqrt{\Delta t} \end{aligned} \quad (\text{E10})$$

$$u_o(n+1) = u_o(n) + \tilde{S}\bar{u}_s(n)(u_a(n) - u_o(n))\Delta t \quad (\text{E11})$$

$$u_o(n+1) = u_o(n) + \tilde{S}\bar{u}_s(n)(u_a(n) - u_o(n))\Delta t. \quad (\text{E12})$$

472 Where  $\zeta_u(n)$  and  $\zeta_v(n)$  are two independent normally distributed centered random variables  
473  $\langle \zeta_u(n)\zeta_u(m) \rangle = \langle \zeta_v(n)\zeta_v(m) \rangle = \delta_{n,m}$ . All random variables are generated by a Mersenne twister.

## 474 References

475 Barrat, J.-L., and J.-P. Hansen, 2003: *Basic concepts for simple and complex liquids*. Cambridge  
476 University Press.

477 Beena, B. S., and J.-S. Von Storch, 2009: Effects of fluctuating daily surface fluxes on the time-  
478 mean oceanic circulation. *Climate dynamics*, **33** (1), 1–18.

479 Boffetta, G., and R. E. Ecke, 2012: Two-dimensional turbulence. *Annual Review of Fluid Mechan-*  
480 *ics*, **44**, 427–451.

481 Csanady, G. T., 2001: *Air-sea interaction: laws and mechanisms*. Cambridge University Press.

482 Duhaut, T. H., and D. N. Straub, 2006: Wind stress dependence on ocean surface velocity: Im-  
483 plications for mechanical energy input to ocean circulation. *Journal of physical oceanography*,  
484 **36** (2), 202–211.

485 Einstein, A., 1906: Zur theorie der brownischen bewegung. *Annalen der Physik*, **324** (2), 371–381.

- 486 Einstein, A., 1956: *Investigations on the Theory of the Brownian Movement*. Courier Corporation.
- 487 Frankignoul, C., and K. Hasselmann, 1977: Stochastic climate models, part ii application to sea-  
488 surface temperature anomalies and thermocline variability. *Tellus*, **29** (4), 289–305.
- 489 Grianik, N., I. Held, K. Smith, and G. Vallis, 2004: The effects of quadratic drag on the inverse  
490 cascade of two-dimensional turbulence. *Physics of Fluids*, **16** (1), 73–78.
- 491 Hasselmann, K., 1976: Stochastic climate models part i. theory. *Tellus*, **28** (6), 473–485.
- 492 Hogg, A. M. C., W. K. Dewar, P. D. Killworth, and J. R. Blundell, 2003: A quasi-geostrophic  
493 coupled model (q-gcm). *Monthly weather review*, **131** (10), 2261–2278.
- 494 Klimontovich, Y. L., 1994: Nonlinear brownian motion. *Physics-Uspokhi*, **37** (8), 737–766.
- 495 Marconi, U. M. B., A. Puglisi, L. Rondoni, and A. Vulpiani, 2008: Fluctuation–dissipation: re-  
496 sponse theory in statistical physics. *Physics reports*, **461** (4), 111–195.
- 497 Moulin, A., and A. Wirth, 2014: A drag-induced barotropic instability in air–sea interaction.  
498 *Journal of Physical Oceanography*, **44** (2), 733–741.
- 499 Moulin, A., and A. Wirth, 2016: Momentum transfer between an atmospheric and an oceanic layer  
500 at the synoptic and the mesoscale: An idealized numerical study. *Boundary-Layer Meteorology*,  
501 **160** (3), 551–568.
- 502 Perrin, J., 2014: *Atomes (Les)*. CNRS Editions, Paris, ISBN: 978-2-271-08260-2, 308 pp.
- 503 Platen, E., 1999: An introduction to numerical methods for stochastic differential equations. *Acta*  
504 *numerica*, **8**, 197–246.
- 505 Risken, H., 1996: Fokker-planck equation. *The Fokker-Planck Equation*, Springer, 63–95.

- 506 Stull, R. B., 2012: *An introduction to boundary layer meteorology*, Vol. 13. Springer Science &  
507 Business Media.
- 508 Vallis, G. K., 2017: *Atmospheric and oceanic fluid dynamics*. Cambridge University Press.
- 509 Williams, P. D., 2012: Climatic impacts of stochastic fluctuations in air–sea fluxes. *Geophysical*  
510 *Research Letters*, **39** (10).

511 **LIST OF TABLES**

512 **Table 1.** Numerical results from the integration of the 2D model. The best fit and the  
513 corresponding standard error of the growth of the second-order moments of the  
514 atmosphere the ocean and the correlation between the two is given (obtained  
515 through xmgrace software). For  $c = 1$  the values correspond to the data and fit  
516 shown in fig. 3. . . . . 32

517 **Table 2.** Numerical results from the integration of the 2D model. Results are differences  
518 of second order moments, which are stationary following the theory developed  
519 for the local models. . . . . 33

520 **Table 3.** Results of the diagnosed parameters compared to the true values are presented:  
521  $\tilde{S} = 10^{-3}$  is the prescribed stability parameter and  $M = m + 1$ , with  $m = 100$  the  
522 mass ratio between the ocean and the atmospheric layer. Parameters calculated  
523 theoretically are:  $S_{\text{obs}}$  is obtained through eq. (37),  $S_{\text{lin}}$  is obtained through eq.  
524 (38),  $M_{\text{obs}}$  obtained through eq. (39) and  $M_{\text{lin}}$  is obtained through eq. (40). . . . . 34

c	$\partial_t \langle \mathbf{u}_a^2 \rangle$	$\partial_t \langle \mathbf{u}_a \mathbf{u}_o \rangle$	$\partial_t \langle \mathbf{u}_o^2 \rangle$
1	$6.78\text{e-}04 \pm 2.41\text{e-}04$	$2.92\text{e-}05 \pm 8.2\text{e-}06$	$3.839\text{e-}05 \pm 1.29\text{e-}07$
8	$6.71\text{e-}04 \pm 2.37\text{e-}04$	$2.95\text{e-}05 \pm 8.2\text{e-}06$	$3.842\text{e-}05 \pm 1.26\text{e-}07$
64	$6.63\text{e-}04 \pm 1.79\text{e-}04$	$3.06\text{e-}05 \pm 7.7\text{e-}06$	$3.580\text{e-}05 \pm 8.2\text{e-}08$
256	$4.66\text{e-}04 \pm 1.74\text{e-}04$	$2.47\text{e-}05 \pm 5.5\text{e-}06$	$2.053\text{e-}05 \pm 1.2\text{e-}07$
1024	$2.8\text{e-}05 \pm 3.3\text{e-}05$	$2.13\text{e-}06 \pm 8.4\text{e-}07$	$2.085\text{e-}06 \pm 4.1\text{e-}08$

525 TABLE 1. Numerical results from the integration of the 2D model. The best fit and the corresponding standard  
526 error of the growth of the second-order moments of the atmosphere the ocean and the correlation between the  
527 two is given (obtained through xmgrace software). For  $c = 1$  the values correspond to the data and fit shown in  
528 fig. 3.

c	$\langle \mathbf{u}_a \mathbf{u}_o - \mathbf{u}_o^2 \rangle$	$\langle (\mathbf{u}_a - \mathbf{u}_o)^2 \rangle$	$\langle (\sqrt{(\mathbf{u}_a - \mathbf{u}_o)^2} (\mathbf{u}_a \mathbf{u}_o - \mathbf{u}_o^2)) \rangle$	$\langle \sqrt{(\mathbf{u}_a - \mathbf{u}_o)^2}^3 \rangle$
1	5.34e-03	9.26	2.09e-02	36.9
8	5.30e-03	9.09	2.06e-02	35.8
64	4.31e-03	5.27	1.29e-02	15.5
256	1.69e-03	0.943	2.09e-03	1.18
1024	1.53e-04	3.11e-02	3.70e-05	7.17e-03

529 TABLE 2. Numerical results from the integration of the 2D model. Results are differences of second order  
530 moments, which are stationary following the theory developed for the local models.

c	$S_{\text{obs}}/\tilde{S}$	$S_{\text{lin}}/\tilde{S}$	$M_{\text{obs}}/M$	$M_{\text{lin}}/M$
1	0.92	0.95	17	17
8	0.93	0.96	17	17
64	1.4	1.5	12	12
256	4.9	5.0	5.6	5.5
1024	28	31	1.9	2.0

531 TABLE 3. Results of the diagnosed parameters compared to the true values are presented:  $\tilde{S} = 10^{-3}$  is the pre-  
532 scribed stability parameter and  $M = m + 1$ , with  $m = 100$  the mass ratio between the ocean and the atmospheric  
533 layer. Parameters calculated theoretically are:  $S_{\text{obs}}$  is obtained through eq. (37),  $S_{\text{lin}}$  is obtained through eq. (38),  
534  $M_{\text{obs}}$  obtained through eq. (39) and  $M_{\text{lin}}$  is obtained through eq. (40).

535

## LIST OF FIGURES

536

537

538

539

540

541

**Fig. 1.** The figures represent a comparison of the analytic (dotted line), the linear (cubes) and the nonlinear model (full line) for the velocity variance in the atmosphere (black) and the ocean (green) and the covariance of the atmosphere and the ocean (red). Right figure is a zoom. The parameters in the linear model are ( $M = 101, S = 2.485 \cdot 10^{-3}, R = 0.5$ ) and in the nonlinear model are ( $M = 101, \tilde{S} = 10^{-3}, R = 0.5$ ). The dotted lines mostly disappear behind the corresponding (same color) full lines. . . . . 36

542

543

544

**Fig. 2.** Vorticity in the atmosphere (top, color-bar ranges from [-850,850]) and the ocean (bottom, color-bar ranges from [-4,4]) over a square with side-length one (total domain spans  $10 \times 10$ ). . . . . 37

545

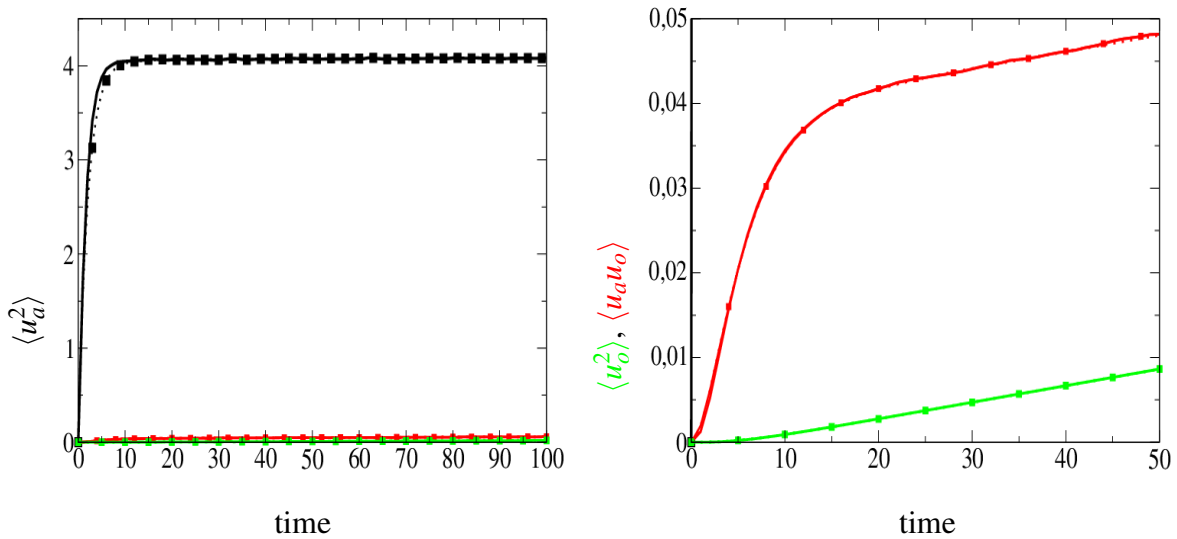
546

547

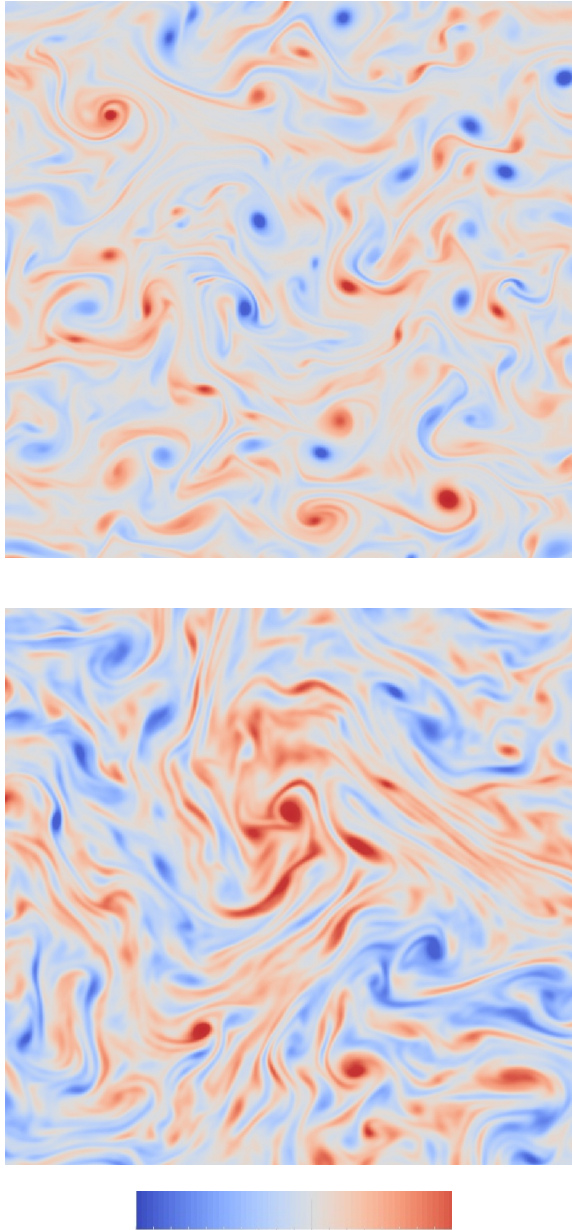
548

549

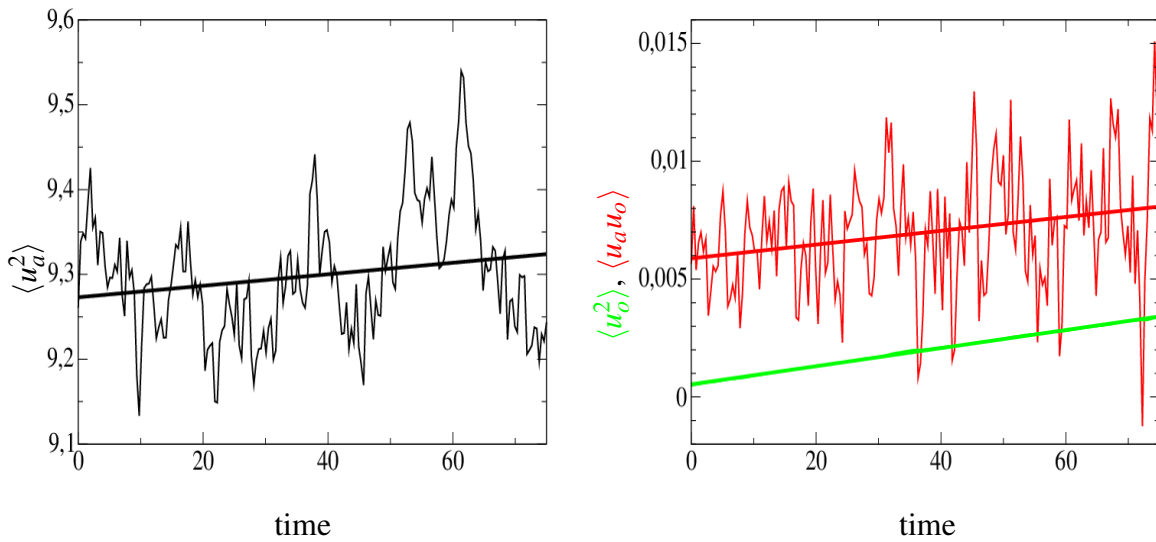
**Fig. 3.** The figures represent results from the 2D simulations (thin lines) and the corresponding linear regression (thick lines, the values of the fit and the uncertainties are given in tab. 3): the atmospheric variance ( $\langle u_a^2 \rangle$ , black, left) and the covariance between the atmosphere and the ocean ( $\langle u_a u_o \rangle$ , red, right) and the oceanic variance ( $\langle u_o^2 \rangle$ , green, right). For the ocean case the thick line superposes the thin line. . . . . 38



550 FIG. 1. The figures represent a comparison of the analytic (dotted line), the linear (cubes) and the nonlinear  
 551 model (full line) for the velocity variance in the atmosphere (black) and the ocean (green) and the covariance  
 552 of the atmosphere and the ocean (red). Right figure is a zoom. The parameters in the linear model are ( $M =$   
 553  $101, S = 2.485 \cdot 10^{-3}, R = 0.5$ ) and in the non-linear model are ( $M = 101, \tilde{S} = 10^{-3}, R = 0.5$ ). The dotted lines  
 554 mostly disappear behind the corresponding (same color) full lines.



555 FIG. 2. Vorticity in the atmosphere (top, color-bar ranges from  $[-850, 850]$ ) and the ocean (bottom, color-bar  
556 ranges from  $[-4, 4]$ ) over a square with side-length one (total domain spans  $10 \times 10$ ).



557 FIG. 3. The figures represent results from the 2D simulations (thin lines) and the corresponding linear re-  
 558 gression (thick lines, the values of the fit and the uncertainties are given in tab. 3): the atmospheric variance  
 559 ( $\langle u_a^2 \rangle$ , black, left) and the covariance between the atmosphere and the ocean ( $\langle u_a u_o \rangle$ , red, right) and the oceanic  
 560 variance ( $\langle u_o^2 \rangle$ , green, right). For the ocean case the thick line superposes the thin line.